



Modelling ADS-B Reception Probability Using OpenSky Data

Muhammad Fazlur Rahman ^{*}, Joost Ellerbroek , and Jacco Hoekstra

Faculty of Aerospace Engineering, Delft University of Technology, Delft, Netherlands

*Corresponding author: m.f.rahman@tudelft.nl

(Received: 31 Oct 2024; Revised: 23 May 2025 and 30 Sep 2025; Accepted: 16 Oct 2025; Published: 31 Oct 2025)

(Editor: Martin Strohmeier; Reviewers: Vincent Lenders, Matthias Schäfer)

Abstract

This paper introduces a model for estimating ADS-B (Automatic Dependent Surveillance-Broadcast) reception probability based on OpenSky network data. The methodology derives reception probability from the distribution of ADS-B message update intervals by examining variations in interval "bumps" around the 0.5-second transmission frequency, shaped by system jitter. Only sensors with circular coverage are used to ensure uniform reception probability estimation. Key variables such as distance, air traffic, and airport interference are binned and used in regression analysis to estimate model constants. Results demonstrate that this model achieves a lower Root Mean Square Error (RMSE) compared to Chung's model, indicating higher accuracy. However, challenges remain in capturing complex interactions between distance, traffic, and airports in proximity, partly due to unmodeled interdependencies and these features serve as proxies to the dependent variable. Further investigation of these relationships could enhance the model's depiction of ADS-B reception probability.

Keywords: ADS-B, Update Interval, Reception Probability Model, OpenSky

Abbreviations: ADS-B: Automatic Dependent Surveillance-Broadcast, ATM: Air Traffic Management, ATCRBS: Air Traffic Control Radar Beacon System, FRUIT: False Replies Unsynchronized in Time, RMSE: Root Mean Square Error

1. Introduction

ADS-B is a surveillance technology that enables aircraft to automatically broadcast detailed flight information, such as GPS position and ground speed. It has been available since the development of Mode S Extended Squitter in the 2000s, an advancement from earlier systems like the Air Traffic Control Radar Beacon System (ATCRBS) [1]. This marked a significant improvement over previous technologies by allowing for more precise and frequent data transmission, which is crucial for managing increasing air traffic volumes. Since then, studies such as [2, 3, 4] have evaluated the performance of the ADS-B system. Additionally, networks like OpenSky now provide public access to global ADS-B data [5], supporting collective ADS-B receiver studies such as those in [6].

As a surveillance system, ADS-B offers numerous possibilities for innovation in air traffic management, including applications like airborne self-separation, which has been extensively studied since the 1990s [7]. However, despite its advantages, ADS-B also presents certain limitations that can impact its effectiveness and reliability in various operational scenarios. These limitations are particularly important to consider as air traffic continues to grow and the demand for more efficient surveillance systems increases.

The limitations of ADS-B primarily arise from factors such as reception probability, signal interfer-

ence, and the dependency on accurate data broadcasting by aircraft. Reception probability refers to the likelihood that an ADS-B signal transmitted by an aircraft is successfully received by ground stations or other aircraft, which can be affected by distance and interference. Signal interference, both from similar frequency usage and overlapping ADS-B transmissions, can lead to potential message loss and garbling [8, 9]. Additionally, the reliance on aircraft to broadcast precise and timely data means that any discrepancies or delays in transmission can result in increased uncertainty in surveillance coverage and aircraft separation. These sources of limitations can lead to issues like data loss, increased uncertainty in aircraft positioning, and potential vulnerabilities in surveillance coverage, which are critical considerations for the overall performance of the ADS-B system.

To investigate these limitations, studies such as those conducted by Langejan [10] and Idris [11] have modeled and analyzed the influence of ADS-B characteristics on self-separation performance. These studies utilize the reception probability model proposed by Chung [12], which, while widely used in simulations, has certain limitations regarding its verification under diverse traffic and Air Traffic Control (ATC) conditions. Specifically, Chung’s model has been verified primarily under a single traffic and surrounding ATC scenario, which may not fully capture the variability and complexity of real-world air traffic environments. Additionally, some parameters within the model, derived from technical specifications [13], may not accurately reflect actual operational conditions, potentially affecting the reliability of the simulation outcomes.

To evaluate the accuracy of the proposed model, this paper is structured as follows. Section 2 provides an overview of the ADS-B system, offering context for the discussion of reception probability modelling. In Section 3, we present both Chung’s existing model and the proposed alternatives. The methodology used to estimate reception probability and develop the new model using OpenSky data is described in detail in Section 4. Following that, results from this analysis are presented in Section 5, followed by a comprehensive discussion in Section 6, where the performance of both models is compared. Finally, Section 7 concludes the study, summarizing key findings and their implications for future research.

2. ADS-B Overview

ADS-B operates using the Mode-S Extended Squitter protocol, which enables aircraft to broadcast information periodically without the need for interrogation by ground radar. According to data from the OpenSky network [14], approximately 18% of all Mode-S communication are extended squitter transmissions, which are typically used for ADS-B messages. This system significantly improves situational awareness by transmitting real-time data such as aircraft position, velocity, and identification. Of these, position and velocity are broadcast twice per second, whereas the remaining data are transmitted at lower frequencies.

The reception of ADS-B messages is based on line-of-sight propagation, meaning that any obstruction between the transmitter and the receiver can cause significant signal loss. In an ideal scenario, where there are no obstructions and the transmitter operates at sufficient power, the maximum range of the receiver is constrained by the curvature of the Earth. The maximum detection range (r), as illustrated in Figure 1, is a function of the Earth’s radius (R) and the angular separation between the aircraft’s position and the tangent point on the Earth’s curvature along the line of sight (α_t), as well as the angular separation between the receiver’s position and the tangent point (α_r). This relationship is described in Equation 1, with both α_t and α_r are expressed in radian. From this, the minimum altitude required for an aircraft to be detected at a given range (h_t) can be stated in terms of r , R , and the receiver altitude (h_r) as shown in Equation 2.

$$r = (\alpha_r + \alpha_t)R$$

$$= \left(\arccos\left(\frac{R}{R+h_r}\right) + \arccos\left(\frac{R}{R+h_t}\right) \right) R \quad (1)$$

$$h_t = \frac{R}{\cos\left(\frac{r}{R} - \arccos\left(\frac{R}{R+h_r}\right)\right)} - R \quad (2)$$

Using Equation 2, the relationship between range and the minimum altitude of the aircraft for detection is visualized in Figure 2. Each curve corresponds to a different receiver height, showing how raising the receiver above ground level reduces the required minimum altitude for detection at a given range. The area below the curve represents the blackout zone, where aircraft cannot be detected due to line-of-sight limitations.

For example, at a range of 300 km, an aircraft can only be detected above an altitude of 7.07 km if the receiver is located at ground level (0 m). When the receiver is placed at 300 m elevation, the minimum altitude requirement decreases to 4.45 km. This illustrates that increasing the receiver height extends coverage by lowering the altitude threshold, thereby improving the probability of detecting aircraft at long ranges.

However, line-of-sight is just one factor affecting ADS-B reception; signal strength and interference also play a critical role. To better understand the factors impacting ADS-B message reception, the next subsections will examine two key aspects: the signal power range and the influence of interference on the system.

2.1 Signal Power Range Model

The relationship between transmission range, received signal power, and reception probability is important in understanding the performance of radio communication like ADS-B. The Friis transmission model, shown in Equation 3, shows the ratio between the received and transmitted signal power ($\frac{Pow_r}{Pow_t}$) depends on factors such as the directivities of the receiving (D_r) and transmitting (D_t) antennas, wavelength (λ), and the distance between the receiver and transmitter (d). This means that as the distance increases, the received signal power decreases, leading to a lower signal-to-noise (SNR) ratio.

$$\frac{Pow_r}{Pow_t} = D_t D_r \left(\frac{\lambda}{4\pi d} \right)^2 \quad (3)$$

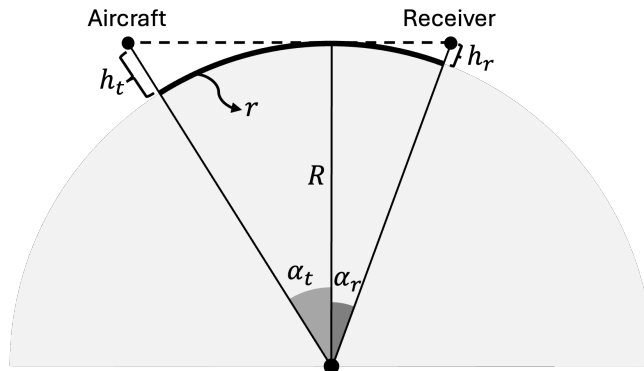


Figure 1. ADS-B maximum distance illustration, adapted from [15].

Consequently, the receiver's ability to separate the signal from the noise reduces, leading to a higher error rate and subsequently lowering reception probability. Studies including those in [8] and [9] have shown that at a greater distance, the SNR is reduced and the message loss and error rate increase. This highlights the importance of considering the distance in the modelling of the reception probability.

2.2 Interference

Interference in the 1090 MHz band is a significant issue due to congestion from multiple surveillance systems. Strohmeier et al. [9] highlight that legacy systems like Mode A/C and Mode S, which were not designed for current traffic levels, continue to operate alongside ADS-B, contributing to problems like False Replies Unsynchronized in Time (FRUIT) where overlapping signals reduce signal quality. The random channel access nature of ADS-B, which lacks coordination, further exacerbates interference during periods of high traffic. Similarly, Sun and Hoekstra [8] found that the combination of Mode S Extended Squitter and legacy Mode A/C systems leads to frequent signal garbling in high-traffic areas, reducing ADS-B message reception. Both studies suggest the current system struggles with increased traffic load, indicating a need for rearrangement for the frequency usage.

Both studies conclude that surrounding air traffic plays a critical role in the congestion of the 1090 MHz band. High aircraft traffic density increases the probability of overlapping transmissions, leading to signal interference and a reduction in ADS-B message reception probability. Additionally, Mode A/C signals, which originate from airports as they interrogate nearby aircraft, contribute significantly to this congestion. Therefore, both air traffic and the number of nearby airports are considered in our model, as these variables directly influence the level of signal congestion and the resulting decrease in ADS-B reception probability.

3. Reception Probability Formulation

The study from [4] finds that the average update interval of received position data from an ADS-B message increases with rising air traffic density due to channel congestion. As more aircraft transmit on the same frequency, signal interference becomes more likely, leading to missed messages and longer intervals between received position updates [8].

While this study provides valuable insights into the relationship between update intervals and traffic, the use of the average update interval to quantify message reception has limitations. ADS-B transponders nominally transmit position messages with a period of 0.5 seconds, but jitter or random offset causes the actual intervals to deviate around this value. As a result, changes in the average update interval do not adequately capture the behaviour of ADS-B message reception. We therefore

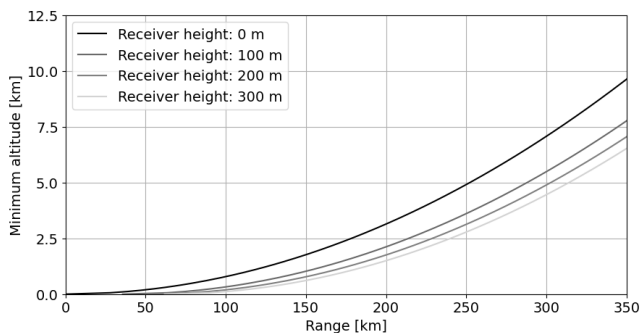


Figure 2. Minimum Detection Altitude

propose to describe reception performance in terms of the probability of successfully receiving a message, hereafter referred to as the reception probability.

First, let us discuss the probability model. Assume the probability of successfully receiving a message at a ground receiver follows an independent Bernoulli trial, where p represents the reception probability. The number of trials required for the first successful reception follows a geometric distribution, with the probability mass function (PMF) given in (4). Here, p is the success probability in each trial, and $(1 - p)^{i-1}$ represents the probability of experiencing $i - 1$ failures before the first success, with i denoting the number of trials until the first success.

$$P(X = i) = p(1 - p)^{i-1} \quad (4)$$

Figure 3 shows a sample histogram of the update interval from a receiver in Delft. The same pattern is also observed in [4]. Two characteristics are visible in this graph. The first is the 'bumps' around multiples of 0.5 seconds, the transmission period. Next is the 'spread' around each multiple of the transmission period. The spread can be explained by the jitter in the transmission time, which consists of a uniform jitter imposed in the design as explained in [16] and a naturally occurring random jitter [17]. Should this jitter be removed, the time interval will be exactly every 0.5 seconds.

To estimate the reception probability, we assume that the jitter causes the transmission times to deviate within the interval 0.25 to 0.75 seconds. Under this assumption, each bump in the histogram spans a fixed 0.5-second window. The reception probability is then obtained by evaluating the area of the first bump relative to the total area of the histogram. In the example of Figure 3, this first bump constitutes 69.23% of the total, followed by the second bump at 21.3%.

For subsequent bumps, deviations become more apparent: the third bump is observed at 6.55% while the model predicts 3.80%, and the fourth at 2.02% compared to 3.39%. Similarly, the fifth and sixth bumps appear at 0.62% and 0.19% in the observation, while the theoretical values are 0.92% and 1.20%, respectively. Overall, the observation can be modeled using the geometric formulation, with good agreement in the first two bumps. Beyond the second bump, however, deviations emerge as the model underestimates the probability mass in the middle tail and slightly overestimates it in the far tail. Nonetheless, the formulation remains sufficiently accurate as an approximation of the reception probability.

3.1 Existing Model

Building on the concept of reception probability introduced earlier, several models have been developed to simulate the reception of ADS-B messages. One widely used model is the 1090 MHz Extended Squitter ADS-B reception model proposed by Chung [12]. This model has been used in research such as [10] and [11] for an air traffic management simulation purposes. It offers a practical approach by taking into account two key factors affecting the reception probability, that are range and interference. While the range between the aircraft and the receiver impacts signal strength, the model also considers interference from other systems operating on the 1090 MHz frequency, particularly Mode A/C, Mode S, and TCAS transmissions.

Another study addressing 1090 MHz interference is presented by Garcia and Taylor in their working paper [18]. Their model focuses on satellite-based ADS-B reception and builds on a Poisson-based framework to evaluate the impact of FRUIT (False Replies Unsynchronized in Time) interference by simulating message overlaps caused by surrounding aircraft. The analysis incorporates aircraft density, satellite antenna gain patterns, and multi-avionics equipage rates to estimate the probability of successful message decoding in orbit. Similarly, an earlier study by Orlando and Harman [19] developed an interference model for GPS-Squitter, a system that also operates on the 1090 MHz frequency,

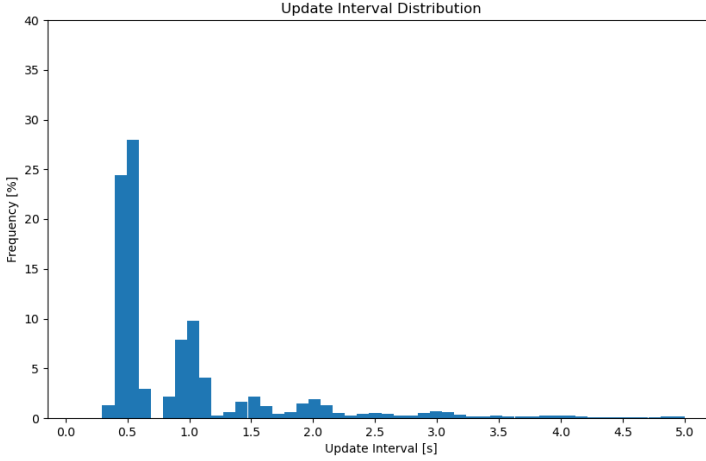


Figure 3. An example of update interval histogram

making it directly comparable in terms of channel occupancy and interference effects. While both models offer detailed and low-level perspectives on interference effects, neither includes distance as a direct variable in the model, limiting their suitability for air traffic management simulations where range-dependent effects are important. Thus, we only consider the model proposed by [12] for comparison.

As discussed previously in [8] and [9], Mode A/C systems, typically used for older transponders, can cause interference known as FRUIT, while Mode S, including its extended squitter variant used by ADS-B, adds further interference due to overlapping messages. The model employs a Poisson distribution to calculate the likelihood of interference from these systems. It adjusts the probability of successfully receiving an ADS-B message based on the number of overlapping signals and the range. As the distance increases, especially in areas with high air traffic density and overlapping transmissions, the likelihood of successful message reception decreases.

$$\begin{aligned}
 p = & d(0) \cdot P(0|m_A) \cdot P(0|m_S) + \\
 & \left[\sum_{x=1}^5 d_A(x) \cdot P(x|m_A) \right] \cdot P(0|m_S) + \\
 & d_S(1) \cdot P(1|m_S) \cdot P(0|m_A) + \\
 & \left[\sum_{x=1}^5 d_A(x) \cdot P(x|m_A) \right] \cdot d_S(1) \cdot P(1|m_S)
 \end{aligned} \tag{5}$$

Equation 5 models the probability p of successfully receiving a 1090ES (ADS-B) message while considering interference from both Mode A/C and Mode S transmissions. Here, x denotes the number of overlaps, the subscript A refers to ATCRBS interference, and S represents Mode S interference. The four terms in the equation represent various interference scenarios.

The first term, $d(0) \cdot P(0|m_A) \cdot P(0|m_S)$, represents the probability of message reception without interference. The second term, $\sum_{x=1}^5 d_A(x) \cdot P(x|m_A) \cdot P(0|m_S)$, accounts for 1 to 5 Mode A/C overlaps with no Mode S interference. The third term, $d_S(1) \cdot P(1|m_S) \cdot P(0|m_A)$, considers 1 Mode S overlap

without Mode A/C interference, and the final term, $\sum_{x=1}^5 d_A(x) \cdot P(x|m_A) \cdot d_S(1) \cdot P(1|m_S)$, captures simultaneous Mode A/C and Mode S interference. This formulation follows the assumption used in [12], and is therefore adopted here without modification.

Each $d(x)$ term denotes the detect/decode probability as a function of range, with $d_A(x)$ and $d_S(1)$ corresponding to Mode A/C and Mode S interference, respectively. The Poisson probability $P(x|m)$ models the likelihood of having x overlaps based on the mean interference overlap m_A or m_S for Mode A/C and Mode S systems. Together, these terms form a comprehensive model that estimates the probability of successful message reception under varying interference conditions.

A key limitation of this model is that the model relies on fixed parameter values derived from technical specifications [13] and controlled test conditions rather than real-world observational data. In particular, it assumes a constant value of the reception decay exponent in the range-dependent detect/decode probability function ($d(0)$, $d_A(x)$, and $d_S(1)$), which governs how rapidly reception probability deteriorates with distance. This assumption may not hold across varying receiver types, or traffic densities. Therefore, in this paper, we treat the exponent as a free parameter and fit it empirically using large-scale data from the OpenSky network. This allows us to more accurately capture the effect of distance on reception probability based on observational data. In this paper, we call this model as Fitted-Chung Model and referring the original one as Chung Model.

3.2 Adapted Model

A different reception probability model has been proposed by [20] for a vehicular ad hoc networks problem. Killat et al. developed their reception probability model through a hybrid approach that integrates simulation and analytical modelling. This was done to overcome the limitations of purely simulation-based models, especially for large-scale studies that involve thousands of vehicles. Simulating such large scenarios would be computationally exhaustive, so the simulations is used to generate data and build a mathematical model, maintaining credibility while reducing computational effort. The study gathered extensive simulation data and used general linear least squares techniques to derive the model. The key input variables of this model were distance between transmitter and receiver and traffic density.

$$p = e^{-3 \cdot \left(\frac{d}{R_{max}}\right)^2} \cdot \left(1 + \sum_{i=1}^4 a_i \left(\frac{d}{R_{max}}\right)^i\right) \quad (6)$$

(6) shows the model proposed in [20]. This model is based on the Nakagami-m distribution, which accounts for the probabilistic nature of radio signal propagation in vehicular environments, contrasting with the deterministic models used in previous studies [21]. The d term in the equation refers to the distance between the transmitter and receiver, while the R_{max} refers to the critical range, in our case the maximum distance of the receiver. The constant a_i is a function of the vehicle in range, which contributes to the interference, and is estimated using a polynomial curve fitting.

This model can be transferred to our problem because both scenarios—vehicular ad hoc networks and ADS-B signal reception—deal with wireless communication in dynamic environments, where signal propagation and interference play critical roles. The use of an empirical approach analytical modelling to estimate reception probabilities, is applicable to ADS-B data as it faces similar challenges of interference, traffic density, and distance.

4. Methods

Aircraft transmit several types of ADS-B messages. These messages include information such as position, velocity, and other aircraft-specific data. Due to the nature of the transmitted data, it is

possible for some message types to appear identical in consecutive transmissions, especially when the data has not changed significantly between intervals. This can present a challenge in differentiating two separate messages during data collection. Position data is used as the distinguishing factor because the chance of receiving identical position messages consecutively for airborne aircraft is extremely low. This approach effectively filters out duplicate messages and prevents miscalculations for the update intervals.

When an aircraft sends a position message, it can be received by multiple receivers, and each receiver logs the data to OpenSky's position database. Since the reception probability is based on the update interval between consecutive messages, it is crucial to track the timing separately for each individual receiver. This is why we use the time data associated with a specific sensor's serial ID from the sensors column. Given that these sensors are not synchronized, using the local timing from each receiver ensures a more accurate reception probability calculation.

The data for this study was collected for the year of 2022 from the OpenSky database. The receivers used in this research were registered in the OpenSky database, with a total of 2,929 receivers providing coverage across Europe. Although receivers collectively cover the entire area, individual receivers are often subject to obstacles in their line of sight to certain aircraft, which can limit the maximum range and reduce ADS-B message reception. By assuming the horizontal coverage of an ADS-B receiver is circular and addressing challenges of obstacles in the line of sight, a filtering process was applied to the collected data to ensure only sensors that have circular coverage are considered in the modelling.

Although this filtering step reduces the generality of the model, it is essential. Without it, modeling would be nearly impossible due to the open-ended nature of the problem. Sensors with non-circular coverage have varying reception probabilities depending on the direction and distance, making it difficult to establish a consistent model. Additionally, terrain obstructions create unique coverage patterns for each sensor, further complicating generalization. Therefore, we include only sensors with circular coverage in the modeling process, ensuring that the model remains valid for receivers meeting this criterion.

Next, we detail the Sensor Coverage Filtering techniques, which ensures uniform coverage across each receiver. Afterward, we present the Data Processing phase, where the reception probability is binned based on aircraft traffic density and distance. Finally, we introduce the regression techniques used to model ADS-B reception probability and the metrics applied to evaluate the model's fit and accuracy.

4.1 Sensor Coverage Filtering

This filtering process ensures that the sensor coverage from each receiver is as evenly distributed as possible. By constructing a convex hull from the recorded aircraft positions, we can evaluate how closely the coverage approximates a circular shape. This is critical because the maximum distance plays a role in the reception probability equation, so coverage must be as uniform as possible in all directions to maintain accuracy.

$$C = \frac{4 \cdot \pi \cdot Area}{Perimeter^2} \quad (7)$$

To assess how closely the convex hull approximates a circle, three key metrics are used. The first metric is circularity (C), which is derived from the isoperimetric inequality [22]. This inequality states that among all shapes with the same perimeter, the circle encloses the maximum area. Mathematically, circularity is calculated as shown in Equation 7, where a value of 1 indicates a perfect circle. For a convex hull, the area can be computed using computational geometry techniques, while

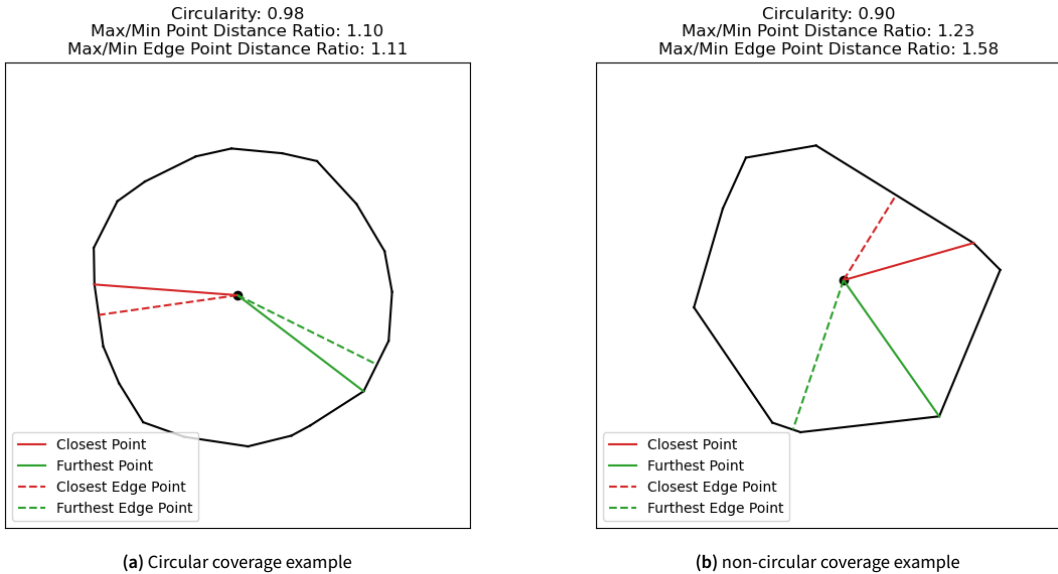


Figure 4. Illustration of the metrics on a circular and non-circular coverage. Note that both the figures have circularity higher than 0.8 and the point distance ratios are less than 1.25. However, for the non-circular image, the edge point distance ratio is higher than 1.25, representing a possibility of a short distance edge.

the perimeter is obtained by summing the Euclidean distances between consecutive hull vertices. Any deviation from this value signifies how much the shape differs from being a circle. Thus, the closer the circularity value is to 1, the more consistent the receiver's coverage across all directions.

While circularity provides a measure of the overall shape of the coverage, it is not sufficient on its own to fully assess the performance of a sensor. Additional metrics are necessary to further evaluate the coverage relative to the receiver location. We therefore propose the second and third metrics, which focus on distance ratios. The second metric compares the distances between the sensor location and the farthest and nearest points on the convex hull, giving insight into how symmetrical the coverage is around the receiver. The third metric evaluates the ratio of distances from the sensor to the farthest and nearest edges of the convex hull. These two distance-based metrics offer a more precise evaluation of how evenly the coverage extends in different directions. For example, a value close to 1 in both metrics would suggest the coverage is nearly uniform, while larger deviations may indicate areas where coverage is weaker due to obstacles or other factors. In this paper, we set specific thresholds for these metrics to determine acceptable coverage quality. A minimum circularity of 0.8 is required, while the distance ratios for the second and third metrics must be less than 1.25 to ensure balanced sensor coverage. These thresholds are a trade-off, chosen loosely close to 1 to allow more receivers to meet the criteria without significantly compromising the circular pattern of the coverage.

Figure 4 shows examples of the three metrics for two different shapes. On the left, the circular coverage example clearly poses a circular shape and supported with the three metrics are within the requirement. On the other side, the non-circular coverage example has a circularity and point distance ratio within the requirement, but the edge point distance ratio is over the limit. This highlights the importance of the third metric, as the shape exhibits a flattened edge on one side, potentially caused by obstacles in the line of sight that limit the coverage of the sensor.

4.2 Data Processing

With the sensor coverage filtering criteria established, we focus exclusively on data from sensors with circular coverage. Key variables, including the aircraft's distance from the sensor, traffic volume, airport interference, and maximum range, are calculated. The distance between the aircraft and the sensor is determined using their respective latitude and longitude coordinates. Traffic volume, defined as the number of aircraft within the coverage area, is quantified by counting unique ICAO codes over one-minute intervals. Airport interference is assessed by counting the number of large and medium airports within the sensor's coverage area. The maximum range is identified as the farthest distance recorded within the sensor's coverage.

Following these calculations, it is necessary to discretize the distance and traffic data into bins. This discretization is crucial because the reception probability is estimated by evaluating the area of the initial "bump" in the update interval histogram relative to the total area. To ensure a representative estimate of the update interval, a sufficiently large sample size is required. A continuous distance-traffic pair are less likely to meet this requirement.

To determine the minimum number of data points required for each distance-traffic bin, we perform a bootstrapping sampling for reception probability with 100,000 data points. Five different numbers of samples are used, 500, 1,000, 2,500, 5,000, and 10,000. Then, we compare the convergence of the reception probability by evaluating the mean and standard deviation for each number of samples. This threshold is important since data availability varies across different distances and traffic bins and is especially sparse near the maximum distance due to limitation by line of sight.

Another important feature for the reception probability estimation is the number of airports within range of the receiver. As suggested in [8], the interference caused by Mode A/C is prevalent in ADS-B reception. For this purpose, we calculate the number of airports that contribute to interference considering the airports within the coverage of the sensors. The airports considered in this research are those of medium and large airports with scheduled service. The number of airports is then determined by considering airports that are within the convex hull of the sensor coverage¹. With the distance, traffic, and number of airports calculated, and the establishment of minimum data requirement, we can calculate the reception probability for each distance-traffic bin and perform a regression analysis.

4.3 Regression and Model Comparison

To reliably estimate the ADS-B reception probability, a curve fitting approach is used. This method allows us to model the relationship between reception probability and key variables such as distance, traffic levels, and the number of airports within the coverage area of the sensor. We use curve fitting because of its flexibility in accommodating the complex, non-linear interactions between these variables, where it provides a more accurate representation of the observed data patterns. The curve fitting is applied to both Fitted-Chung model and the adapted model.

To develop the Fitted-Chung model, we maintain the core structure of Chung's original formulation while treating the decay exponent k as an empirical parameter. The fitted constants appear in Equations (8), (9), and (10), each representing the probability of successfully decoding an ADS-B message under different interference scenarios. In these equations, r denotes the distance between the transmitting aircraft and the receiver, r_0 is the critical range beyond which reception probability falls to zero, and k characterizes the rate of signal degradation with distance. In total, six parameters are fitted to capture the range-dependent decay behavior under varying interference conditions.

¹Available at <https://ourairports.com/data/>

$$d(0) = 1 - \left(\frac{r}{r_0}\right)^k \quad \text{for } r \leq r_0 \quad (8)$$

$$d_A(x) = 1 - \left(\frac{r}{r_0(x)}\right)^{k(x)} \quad \text{for } x = 1, \dots, 5 \quad (9)$$

$$d_S(1) = 1 - \left(\frac{r}{r'_0}\right)^k \quad \text{for } r \leq r'_0 \quad (10)$$

Next, the constants in (6) are empirically fitted from the data. Each coefficient a_i in the model is expressed as a linear function of the number of aircraft (traffic) and airports within the receiver's coverage area, as defined in (11). This formulation allows the model to account for the influence of both traffic density and potential interference from nearby airports. In total, twelve parameters are estimated in this model to capture the combined effects of distance, traffic, and airport-related interference on reception probability.

$$a_i = a_{iT} \cdot \text{traffic} + a_{iA} \cdot \text{airport} + a_{i0} \quad (11)$$

For model validation, the dataset is split into training and testing subsets. The training data is used to fit the model, while a separate sensor with different maximum range and airport is used as the testing data to validate the regression performance, ensuring that the model generalizes well to new, out-of-training parameters. Root Mean Square Error (RMSE) is used as the performance metric to evaluate the accuracy of the regression model.

In addition to single-sensor testing, a cross-validation procedure is carried out across multiple sensors of the same receiver type. In this setup, the model is trained on data from all but one sensor, with the remaining sensor used for testing. This process is repeated for each sensor, allowing a comprehensive evaluation of the model's performance across different sensor environments and coverage profiles. By evaluating the RMSE across folds, we assess how consistently the model performs and identify sensors with relatively higher or lower estimation accuracy. Lastly, the adapted model is compared to the model presented in [12] to assess its relative performance.

5. Results

5.1 Sensor Coverage Filtering

In total, there are more than 5,000 receivers available in OpenSky database and around 2,000 of them are located in Europe. The filtering criteria are then applied to those receivers in Europe by considering data in the first 3 days of June 2022. This results in only 23 receivers fulfilling the circularity and distance ratio characteristics.

Figure 5 illustrates the outcome of the sensor coverage filtering process used to select sensors with more uniform and circular coverage. For illustration purposes, the distance of each vertex in the convex hull is normalized with respect to the maximum distance. Then, the sensor locations are translated into a single point in the middle of the figure.

In subfigure 5a, the circular coverage samples represent sensors that meet the criteria for circularity and balanced distance ratios. These sensors show a more consistent coverage area around the sensor location (marked by the blue dot), with minimal variation in reach across different directions. This

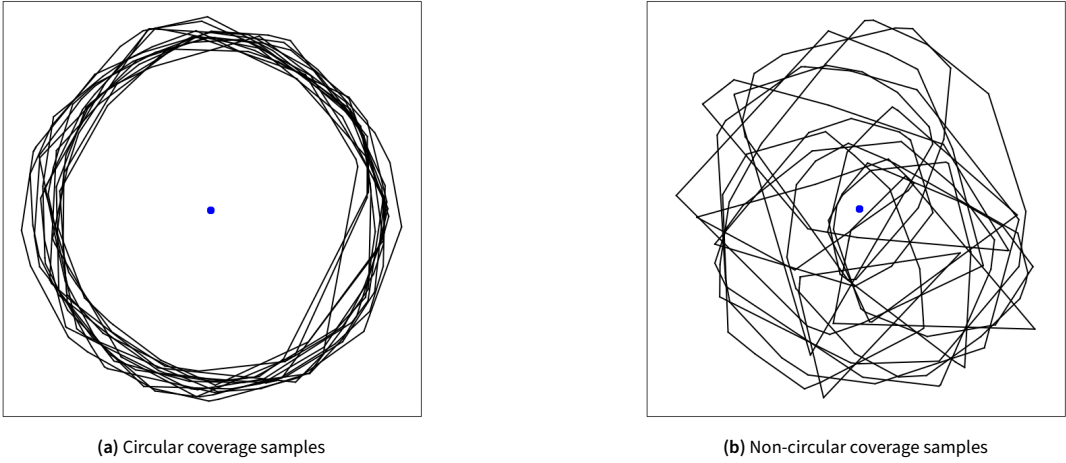


Figure 5. Comparison of sensor coverage after applying the coverage filtering process. (a) Circular coverage samples, (b) Non-circular coverage samples. The blue dots indicate the sensor locations.

uniformity ensures that the data from these sensors provide a reliable basis for modelling reception probabilities, as their range is evenly distributed.

In contrast, subfigure 5b shows non-circular coverage samples, which do not meet the filtering requirements. These sensors exhibit irregular shapes, with coverage that extends unevenly in some directions while being limited in others. Such variations can be caused by obstacles, terrain, or other environmental factors that interfere with signal propagation. By excluding these non-circular samples from the analysis, we eliminate the effects of line-of-sight limitations due to terrain or obstacle occlusion, allowing us to isolate the impact of distance and signal interference from other transmissions.

5.2 Data Processing

Figure 6 shows the distribution of data points across different distance and traffic bins, illustrating the density of ADS-B message receptions with a maximum value limited at 10,000 data points. Darker regions, particularly concentrated in lower distance bins (below 100 km), indicate areas where the majority of messages is successfully received. As expected, the data density decreases with increasing distance, reflecting the challenges posed by greater range. Since the number of data points is not uniform across all distance and traffic bins, a minimum number of data points must be established before estimating the reception probability. This ensures that the results are reliable and not skewed by insufficient data in certain bins.

Figure 7 complements this by illustrating the reception probability across different sample sizes (500, 1000, 2500, 5000, and 10,000 data points). The mean reception probability remains consistent at approximately 0.915 for all sample sizes. However, as the sample size increases, the variability decreases, as shown by the narrowing interquartile range. This reduction in variability reinforces the importance of ensuring adequate sample sizes when estimating reception probabilities, as larger datasets provide more stable and reliable estimates, minimizing the impact of the small sample estimation inaccuracy seen in Figure 6.

To ensure a balanced approach between data coverage and estimation accuracy, the reception probability estimation in this paper will use 2,500 data points. This value is chosen as a compromise between maximizing the number of distance and traffic bin pairs while maintaining a sufficient level of

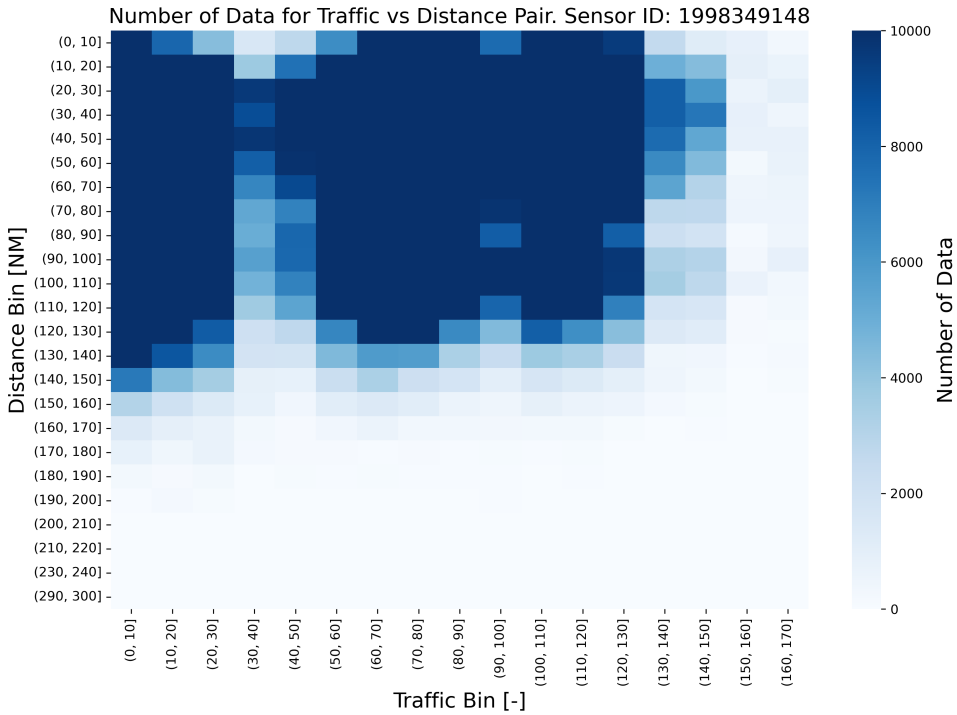


Figure 6. An example of heatmap plot for number of data in different traffic and distance bin pairs

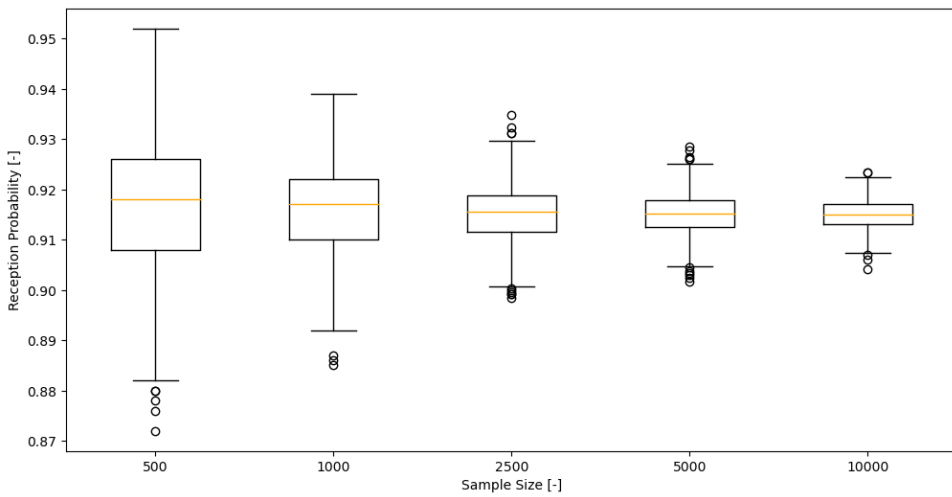


Figure 7. Reception probability across varying sample sizes. The mean reception probability remains approximately 0.915, with standard deviations of 0.012, 0.009, 0.006, 0.004, and 0.003 for sample sizes of 500, 1000, 2500, 5000, and 10,000 data points, respectively.

accuracy in the estimates. Although smaller sample sizes may introduce some variability, as shown in Figure 7, the use of 2,500 data points is considered a balanced choice. Any potential inaccuracies in the reception probability estimation due to smaller sample sizes in certain bins will be addressed through regression modelling, which will correct the deviations. This approach allows the analysis

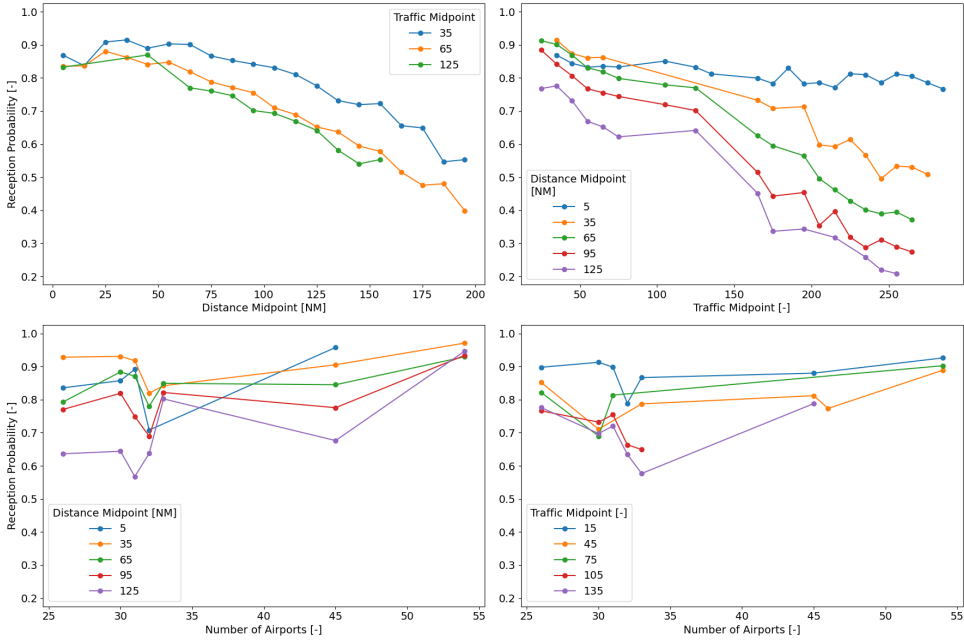


Figure 8. Reception probability as a function of distance (top-left), traffic (top-right), and number of airports (bottom). The results show a decline in reception probability with increasing distance and traffic, while the number of airports introduces variability across different conditions.

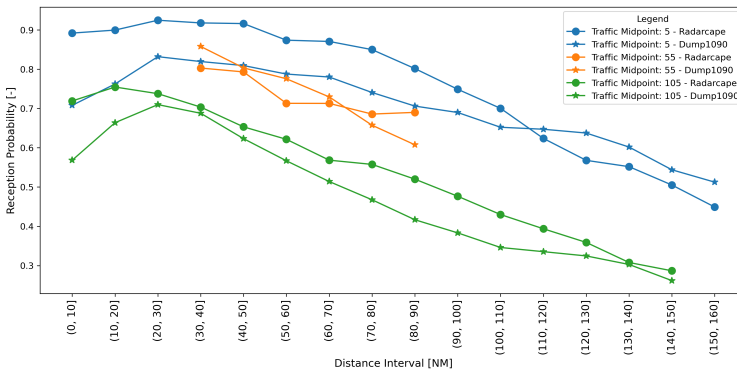


Figure 9. Effect of receiver type on the reception probability. The sensor ID for Radardcape is 1517795776, while for dump1090 is -1408235303.

to capture key trends while managing limitations in data availability across the different bins.

5.3 Effect of Distance, Interference, and Receiver Type

Figure 8 illustrates the effect of range and interference from the number of aircraft and airports within sensor coverage on ADS-B reception probability. In the top subfigures, the data is collected from a single receiver’s coverage, which minimizes the variability in reception probability caused by differences in maximum distance and the number of nearby airports. In contrast, the bottom subfigures present data from sensors with a maximum coverage exceeding 290 NM, showing results at five traffic levels in the bottom-left and for a 15 NM distance midpoint in the bottom-right.

In the top-left plot of Figure 8 it can be seen that reception probability declines significantly as the distance increases, following a second-order polynomial function. This aligns with the Friis transmission model, which predicts that signal strength, and thus reception probability, decreases inversely with the square of the distance. An interesting observation occurs at around 5 NM, where reception probability is lower than the following two data points, a phenomenon also noted in [9]. The main reason for this is the doughnut effect in the reception in close horizontal distance. This effect explains that the signal received along the axis of a dipole antenna, typically used for ADS-B, is significantly less along the antenna axis.

In the top-right plot, reception probability decreases as traffic increases, and the linear trend highlights the clear impact of distance and traffic on reception probability. This is due to the interference caused by other aircraft that use the same 1090 MHz channel.

In the bottom two subfigures of Figure 8, the relationship between reception probability and the number of airports show a more complex, non-linear trend. While it might seem intuitive that a higher number of airports would increase interference due to more Mode A/C and Mode S signals, the plots show that more airports actually correspond to higher reception probability. This observation contrasts with the findings of [8], which noted that increased occupancy of the 1090 MHz frequency can reduce ADS-B message reception.

Lastly, we examine the effect of receiver type on reception probability. Two types of receivers are used in our dataset: Radarcape and dump1090. To ensure a fair comparison, we selected two receivers with similar characteristics in terms of maximum detection range and the number of nearby airports. For Radarcape, sensor ID 1517795776 is selected, with a maximum range of 290 NM and 31 surrounding airports. For dump1090, sensor ID -1408235303 is chosen, with a maximum range of 296 NM and 32 surrounding airports.

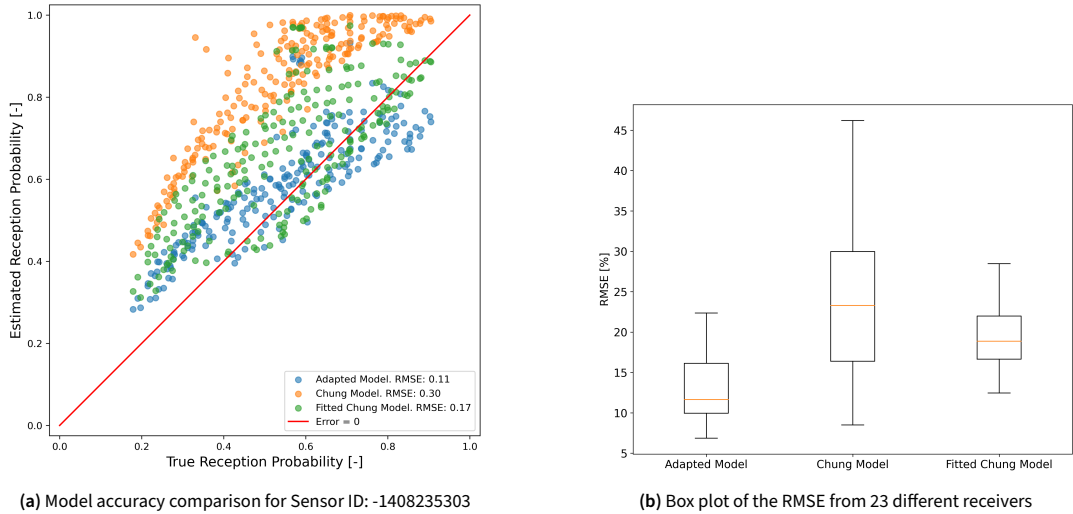
Figure 9 presents the comparison between the two receiver types. Overall, the Radarcape receiver outperforms dump1090 at most distance intervals. However, when the observed traffic is moderate (traffic midpoint 55, corresponding to 50–60 aircraft), the performance gap narrows. This may be attributed to a smaller sample size in this traffic range, which could introduce variability in the reception probability observation.

5.4 Regression and Model Comparison

To model the ADS-B reception probability, a curve-fitting approach was applied to (6) for the adapted model and (8), (9), and (10) for Fitted-Chung model. The regression results are compared between the two models and an Chung model as a benchmark, using both single-sensor evaluation and cross-validation across multiple sensors.

Figure 10a shows a comparison between the adapted model, Chung model, and Fitted-Chung model, evaluated on data from a single receiver. The adapted model comes out as the best fit, with RMSE of 0.11. On the other hand, Fitted-Chung model performs better than the original one with RMSE of 0.17 and 0.30 respectively.

Then, Figure 10b presents the results of a cross-validation performed on 23 different receivers, each is modeled based on receivers of the same type. The adapted model consistently outperforms the existing model, achieving a lower mean RMSE of 13.1%, compared to 23.6% for Chung's model. When the decay exponent k is estimated using curve fitting, the Fitted-Chung model obtains 19.4% mean RMSE across those different receivers. This shows that the estimated reception probability from adapted model is closer to the true reception probability under different range, traffic, geographical condition for different sensors. Therefore, since the best performing model is the adapted model, we further analyze the error in the model associated with the sensor type and distance.



(a) Model accuracy comparison for Sensor ID: -1408235303

(b) Box plot of the RMSE from 23 different receivers

Figure 10. Comparison of the ADS-B reception probability between adapted, Chung model, and Fitted-Chung model.

Next, we analyze the results of the cross-validation regression in more detail to identify which sensor IDs yielded the highest and lowest RMSE values during testing. As shown in Figure 11a, sensor ID -1408235424 produced the highest RMSE, while sensor ID -1408235680 resulted in the lowest RMSE among dump1090 sensors. To understand the factors contributing to this variation, we examine the geographical characteristics of the sensors, such as their maximum detection distance and the number of nearby airports, as illustrated in Figure 11b. Interestingly, the sensor with the highest RMSE is not an outlier. Instead, it is located among other receivers and shares similar geographical features. In contrast, the sensor with the lowest RMSE appears to be more distinct.

Lastly, we assess how estimation accuracy varies across different distance intervals by evaluating the difference between the estimated and the observed reception probability. As shown in Figure 12, the distribution of errors is analyzed alongside the corresponding number of data points for each range. In the 0–20 NM interval, the median error is relatively high at around 8.3%. However, for the 20–120 NM range, the model performs more consistently, with median errors staying between -4.5% to 1.7%, and the standard deviation is between 9.7% to 11.5%, highlighting this range as the most reliable for prediction. Beyond 120 NM, the standard deviation tends to increase, indicating a gradual drop in estimation accuracy with distance. Notably, the final three intervals (180–200 NM, 200–220 NM, and 220–240 NM) contain significantly fewer data points, making their error metrics less robust for comparison.

6. Discussion

The sensor coverage filtering process proved effective in eliminating non-circular sensor coverages. By applying strict circularity and distance ratio criteria, we ensure that only sensors with uniform coverage in all directions are used. This filtering step is crucial for reducing potential inaccuracies caused by uneven coverage, as the estimation of reception probability depends on the maximum distance.

The number of data points required for accurate reception probability estimation is determined to be at least 2,500. This value represents a trade-off between maintaining sufficient coverage of the distance and traffic bins while ensuring estimation accuracy. Although larger sample sizes would

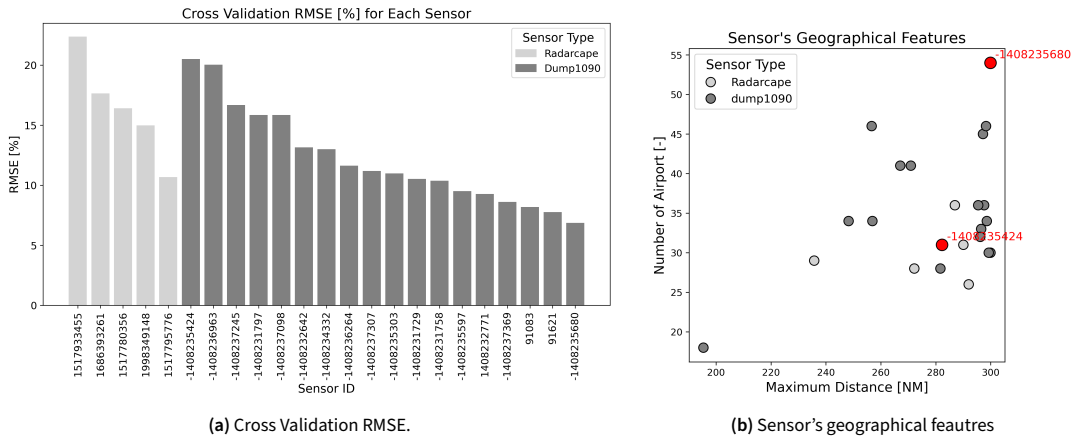


Figure 11. Cross validation RMSE and receiver's geographical features. The regression is done on different receivers to evaluate the model performance on unique conditions.

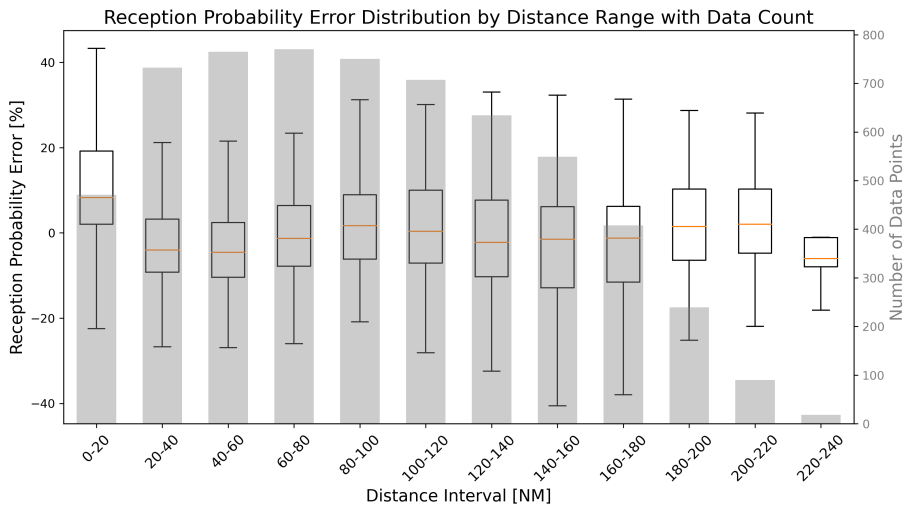


Figure 12. Reception Probability Error Comparison. The regression estimation is more reliable within 20 to 120 NM.

further reduce variability, using 2,500 data points provides a balance between capturing key trends and managing the limited data availability in certain bins.

The effects of distance and traffic on reception probability are evident. As expected, reception probability decreases as distance increases, aligning with the Friis transmission model. On top of that, a higher number of aircraft in the vicinity leads to lower reception probability due to increased frequency interference. However, the effect of the number of airports within a sensor's coverage area is less clear. Surprisingly, receivers covering a greater number of airports exhibit higher reception probabilities. This is because the number of airports serves as a proxy for interference levels rather than a direct measure. Lastly, receiver type also influences reception probability, as seen in the comparison between Radarcape and dump1090 in which former has higher overall reception probability across different distance and traffic situations.

Three models were compared for estimating ADS-B reception probability. The first is the original

Chung model, based on the formulation in [12]. The second, referred to as the Fitted-Chung model, modifies the original by empirically fitting the exponent constants using observed data. Finally, we propose an Adapted model, inspired by the formulation in [21].

Based on the RMSE analysis, the original Chung model performs the worst. This is likely due to its reliance on fixed constants derived from assumptions that may only hold in limited scenarios. In contrast, the Adapted model outperforms both the original and Fitted-Chung models. This improved performance can be attributed to the greater number of fitted parameters, twelve in the Adapted model versus six in the Fitted-Chung model, which provides increased flexibility during regression and enables the model to better capture patterns in the observed data.

Given that the Adapted model achieves the best overall performance, we conducted a more detailed analysis of its sensor-wise cross-validation results to uncover additional insights. The model's accuracy varies across different sensors, with RMSE values spanning a wide range. Interestingly, the sensor with the highest RMSE is not an outlier in terms of geographical characteristics such as maximum distance or airport density. Conversely, the sensor with the lowest RMSE appears distinct. This suggests that performance differences may not be fully explained by the high-level features considered since those are proxies to the receiver's performance. In summary, frequency interference also depends on the number of ground interrogators, which are not necessarily limited to airports. This emphasizes that the features used in this research act as a proxy to the interference level, rather than a direct measure.

In general, we have seen that the adapted model performs best among the three models. However, despite these improvements, the comparison between the true and estimated values suggests that the current model structure may still be insufficient to fully capture the physical phenomena underlying ADS-B message reception. This might be due to a simplification in the constants a_i that modeled an independent relation between the air traffic and airports in proximity as sources of interference. In reality, both variables can correlate due to the interaction between airport and the air traffic, further creating a more complex model. Furthermore, different sources of interference are potentially missing in the modeling. A deeper analysis of the relation between these two variables and other import factors is required.

Further evaluation of the model's performance across distance intervals highlights another limitation. While the model performs well within the 20–120 NM range, where the standard deviation of the estimation error remains below 11.5%, its accuracy degrades beyond this range. This trend indicates that the model's assumptions or structure may be better suited to mid-range estimations. Moreover, the elevated error observed at short distances (0–20 NM) may be attributed to the doughnut effect, which is not fully captured in the model. Future model improvements could include these factors into consideration.

7. Conclusion

At the beginning of this paper, we set out to address the formulation of ADS-B reception probability by analyzing the distribution of update interval values and comparing an existing model with our new model. To ensure accuracy, we included only receivers with circular coverage in constructing our model. Using regression techniques, we estimated the model constants by considering the effects of distance, air traffic, and airport interference on ADS-B message reception. Our findings indicate that the adapted model is more accurate, achieving a lower RMSE than Chung's model, both the original and the fitted one.

However, despite this improvement in RMSE, our model does not fully capture the trends in reception probability as a function of distance, traffic, and number of airports. Further evaluation showed

that the model performs best in the 20–120 NM range, while accuracy degrades at very short and long distances. This may be due to factors such as the doughnut effect not being fully captured. Additionally, features such as number of surrounding aircraft and the number of nearby airports are used as high-level proxies rather than direct measures of the underlying factors that influence reception probability. While they provide useful indications, they may not fully reflect the physical or interference-related conditions affecting ADS-B message reception performance. A more detailed analysis of how these proxies relate to actual interference levels could help refine the modeling of ADS-B reception probability.

For future work that intends to incorporate this regression model into ADS-B communication systems simulation, it is important to account for the model's error or uncertainty. This is particularly important when used in safety-critical applications such as airborne separation or conflict resolution systems.

Acknowledgement

This research has received funding from the EUSPA under the European Union's HORIZON-EUSPA-2021-SPACE No. 101082484 (CERTIFLIGHT). . This publication solely reflects the authors' view and neither the European Union, nor the funding Agency can be held responsible for the information it contains.

Author contributions

Conceptualization (all), Methodology (all), Software (M.F.R), Formal analysis (M.F.R, J.E), Data Curation (M.F.R), Writing – Original Draft (M.F.R, J.E), Writing –Review & Editing (M.F.R, J.E), Visualization (M.F.R)

Open data statement

All data used in this paper is available on OpenSky Network.

The reception probability model resulted from this paper is available on https://github.com/fazlurnu/adsb_reception_model_opensky/tree/main/model as .csv files.

Reproducibility statement

The code, data, and the model of the paper are openly shared on https://github.com/fazlurnu/adsb_reception_model_opensky/

References

- [1] ICAO. *Secondary Surveillance Radar Mode S Advisory Circular*. International Civil Aviation Organization, 1983.
- [2] Busyairah Syd Ali, Arnab Majumdar, Washington Y Ochieng, and Wolfgang Schuster. "ADS-B: the case for London terminal manoeuvring area (LTMA)". In: *Tenth USA/Europe Air Traffic Management Research and Development Seminar (ATM2013)*. 2013.
- [3] AD Panken, WH Harman, CE Rose, AC Drumm, BJ Chludzinski, TR Elder, and TJ Murphy. "Measurements of the 1030 and 1090 MHz environments at JFK international airport". In: *Project Report ATC-390, Lincoln Laboratory Massachusetts Institute of Technology* (2012).
- [4] T Verbraak, Joost Ellerbroek, Junzi Sun, and Jacco Hoekstra. "Large-scale ADS-B data and signal quality analysis". In: *Proceedings of the 12th USA/Europe Air Traffic Management Research and Development Seminar*. 2017.

- [5] Matthias Schäfer, Martin Strohmeier, Vincent Lenders, Ivan Martinovic, and Matthias Wilhelm. “Bringing up OpenSky: A large-scale ADS-B sensor network for research”. In: *IPSN-14 Proceedings of the 13th International Symposium on Information Processing in Sensor Networks*. IEEE. 2014, pp. 83–94.
- [6] Savio Sciancalepore, Saeif Alhazbi, and Roberto Di Pietro. “Reliability of ADS-B communications: Novel insights based on an experimental assessment”. In: *Proceedings of the 34th ACM/SIGAPP Symposium on Applied Computing*. 2019, pp. 2414–2421.
- [7] Jacco M Hoekstra, Ronald NHW van Gent, and Rob CJ Ruigrok. “Designing for safety: the ‘free flight’ air traffic management concept”. In: *Reliability Engineering & System Safety* 75.2 (2002), pp. 215–232.
- [8] Junzi Sun and Jacco M Hoekstra. “Analyzing aircraft surveillance signal quality at the 1090 megahertz radio frequency”. In: *Proceedings of the 9th International Conference for Research in Air Transportation*. 2020.
- [9] Martin Strohmeier, Matthias Schäfer, Vincent Lenders, and Ivan Martinovic. “Realities and challenges of nextgen air traffic management: the case of ADS-B”. In: *IEEE communications magazine* 52.5 (2014), pp. 111–118.
- [10] Thom Langejan, Emmanuel Sunil, Joost Ellerbroek, and Jacco Hoekstra. “Effect of ADS-B characteristics on airborne conflict detection and resolution”. In: *Proceedings of the 6th Sesar Innovation Days* (2016).
- [11] Husni Idris, Maria C Consiglio, and David J Wing. “Surveillance range and interference impacts on self-separation performance”. In: *2011 IEEE AIAA 30th Digital Avionics Systems Conference*. NF1676L-12303. 2011.
- [12] William Chung and Ronald Staab. “A 1090 extended squitter automatic dependent surveillance-Broadcast (ADS-B) reception model for air-traffic-management simulations”. In: *AIAA modeling and simulation technologies conference and exhibit*. 2006, p. 6614.
- [13] RTCA. *Minimum Operational Performance Standards (MOPS) for 1090 MHz Extended Squitter Automatic Dependent Surveillance-Broadcast (ADS-B) and Traffic Information Services-Broadcast (TIS-B)*. Tech. rep. DO-260A. RTCA, Inc., Apr. 2003.
- [14] Matthias Schäfer, Xavier Olive, Martin Strohmeier, Matthew Smith, Ivan Martinovic, and Vincent Lenders. “OpenSky report 2019: Analysing TCAS in the real world using big data”. In: *2019 IEEE/AIAA 38th Digital Avionics Systems Conference (DASC)*. IEEE. 2019, pp. 1–9.
- [15] Junzi Sun. “The 1090 megahertz riddle: a guide to decoding mode s and ads-b signals”. In: *TU Delft OPEN Publishing* (2021).
- [16] ICAO. *Overview of Automatic Dependent Surveillance-Broadcast (ADS-B) Out*. Available at <https://www.icao.int/NACC/Documents/Meetings/2021/ADSB/P01-OverviewADSBOut-ENG.pdf> (2024/02/03).
- [17] Takahiro J Yamaguchi, Kiyotaka Ichiyama, Harry X Hou, and Masahiro Ishida. “A robust method for identifying a deterministic jitter model in a total jitter distribution”. In: *2009 International Test Conference*. IEEE. 2009, pp. 1–10.
- [18] R. Garcia and M. Taylor. *Analysis of Co-channel Interference to Satellite-based Reception of 1090ES ADS-B*. Available at <https://www.icao.int/safety/acp/ACPWGF/FSMP-WG-F-32/> (Accessed: 2025/04/02).
- [19] V. A. Orlando and W. H. Harman. *GPS-Squitter Interference Analysis*. Available at https://www.ll.mit.edu/sites/default/files/publication/doc/2018-12/Orlando_1995_ATC-229_WW-15318.pdf (Accessed: 2025/04/02).
- [20] Moritz Killat, Felix Schmidt-Eisenlohr, Hannes Hartenstein, Christian Rössel, Peter Vortisch, Silja Assenmacher, and Fritz Busch. “Enabling efficient and accurate large-scale simulations of VANETs for vehicular traffic management”. In: *Proceedings of the fourth ACM international workshop on Vehicular ad hoc networks*. 2007, pp. 29–38.

- [21] Moritz Killat and Hannes Hartenstein. “An empirical model for probability of packet reception in vehicular ad hoc networks”. In: *EURASIP Journal on Wireless Communications and Networking* 2009 (2009), pp. 1–12.
- [22] Marcel Berger. *Geometry revealed: a Jacob’s ladder to modern higher geometry*. eng. Heidelberg New York: Springer, 2010. ISBN: 978-3-540-70997-8.